Letter

Observation of chiral-mode domains in a frustrated XY model on optical triangular lattices

Hideki Ozawa,* Ryuta Yamamoto, and Takeshi Fukuhara
RIKEN Center for Quantum Computing (RQC), Wako 351-0198, Japan

(Received 16 April 2023; revised 30 August 2023; accepted 23 October 2023; published 21 November 2023)

We investigated the relaxation and excitation in a frustrated XY model realized by a Bose gas in Floquet-engineered optical triangular lattices. Periodically driving the position of the entire lattice structure enables the sign inversion of tunneling amplitudes, which, in the case of a triangular lattice, results in geometrical frustration of the local phase of wave packets. We revealed that the two spiral phases with chiral modes show significant differences in relaxation time from the initial ferromagnetic phase. While spontaneous symmetry breaking is clearly observed at a slow ramp of the Floquet drive, simultaneous occupation of two ground states often occurs at a fast ramp, which can be attributed to the domain formation of the chiral modes. The interference of the spatially separated chiral modes was observed, using a quantum gas microscope. This work leads to exploring the domain formation mechanism in a system with $\mathrm{U}(1) \times \mathbb{Z}_2$ symmetry.

DOI: 10.1103/PhysRevResearch.5.L042026

Magnetic frustration is an intriguing issue in condensed-matter physics [1,2]. The simplest example is spins with antiferromagnetic interactions in a triangular lattice, in which all adjacent spins cannot align in antiparallel configurations that minimize the interaction energy. Owing to geometrical frustration, conventional magnetic orders are suppressed, giving rise to nontrivial phenomena and phases such as quantum spin liquids [3]. However, theoretical challenges remain, especially for quantum spin systems. In the experimental side, conventional condensed-matter systems are too complex to realize ideal models of frustrated spin systems [4]. Quantum simulators, controllable physical systems that realize target models, including frustrated spin models, are expected to play a significant role in understanding frustration physics. Such studies have been conducted using various platforms including trapped ions [5,6], neutral atoms in optical lattices [7–11] and in optical tweezer arrays [12,13], superconducting annealers [14], and Josephson junction arrays [15].

Two-dimensional fully frustrated XY models, such as the antiferromagnetic XY model on a triangular lattice, have attracted attention in the past decades [16–19]. The main feature of the models is the discrete $\mathbb{Z}_2$ symmetry stemming from twofold degenerate ground states corresponding to the two chiral modes. There have been many controversial discussions on classical spin models because the phase transition associated with the chiral $\mathbb{Z}_2$ symmetry breaking occurs at a temperature very close to the transition temperature corresponding to the breaking of the continuous U(1) symmetry for global spin rotation. Although the transition temperature of the chiral symmetry breaking is slightly higher than the other transition temperature, there is still no clear consensus on the critical behaviors of transitions [20,21]. For quantum spin models, this combined $\mathrm{U}(1) \times \mathbb{Z}_2$ degeneracy might bring about exotic quantum critical phenomena; however, such critical behaviors have not been elucidated.

Quantum simulation of the classical XY spin model has been demonstrated by using ultracold bosonic atoms in an optical triangular lattice [7]. To realize each ground state in the model, the tunneling amplitudes were manipulated by the lattice-shaking technique [22]. While the interference patterns of the ground states have been observed, relaxation and excitation from the initial ferromagnetic state have rarely been studied.

In this study, we focused on this aspect. The tunneling amplitudes J and J' in the optical triangular lattice are independently controlled by modulating two phases ϕ_1 and ϕ_2 of the three lattice beams [Fig. 1(a)]. By varying the time to ramp up the phase modulation amplitudes, we investigated and compared the relaxation times from the initial ferromagnetic phase (F) to two frustrated phases (Sp1 and Sp2). We combined the lattice-shaking technique with a quantum gas microscope, which has a single-site resolution and single-atom sensitivity [Fig. 1(b)]. This experimental system is capable of investigating phase separation and density waves arising from exotic phases such as lattice supersolidity [23–25].

First, we describe our experimental setup. A sample was prepared by loading a Bose-Einstein condensate (BEC) of ^{87}Rb atoms into a lattice system consisting of an optical triangular lattice and crossed far-off resonance traps (FORTs). The optical triangular lattice potential is given by

$$V(\boldsymbol{r}) = -\frac{V_0}{2}[\cos(\boldsymbol{b}_1 \cdot \boldsymbol{r} + \phi_{23}) + \cos(\boldsymbol{b}_2 \cdot \boldsymbol{r} + \phi_{31}) + \cos(\boldsymbol{b}_3 \cdot \boldsymbol{r} + \phi_{12})] + \frac{1}{2} m\omega_z^2 z^2, \quad (1)$$

*hideki.ozawa@riken.jp

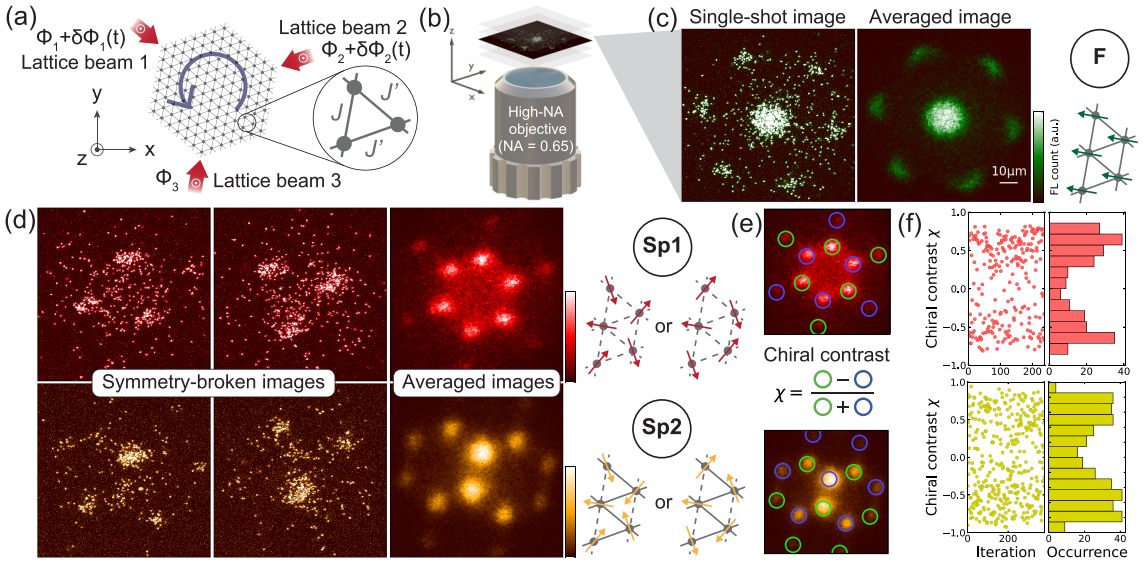

FIG. 1. Schematic of shaken optical triangular lattice and realization of the XY spin model. (a) The tunneling parameters J and J' can be tuned independently by modulating the phase of two lattice beams. (b) Observation with the quantum gas microscope. The samples are loaded into a vertical lattice, and the single layer located at the microscope's focus is selectively detected by removing atoms in the other layers before the measurement. (c) Observation of a ferromagnetic phase (F). Color bars indicate fluorescent (FL) counts. Arrows on the rightmost sketch mean the spin state. (d) Observation of spontaneous symmetry breaking in two phases with frustration: Spiral 1 (Sp1) and Spiral 2 (Sp2). The two columns on the left show the single-shot symmetry-broken images with different chiral modes. For the averaged images in panels (c) and (d), 20 and 100 independent experimental realizations were used, respectively. The solid (dashed) lines in the rightmost column mean tunnelings with positive (negative) signs. (e) Definition of chiral contrast χ, which indicates chiral order. (f) Statistical distributions (left) and histograms (right) of χ for Sp1 and Sp2.

where V_0 is the lattice depth, $\boldsymbol{b}_i$ is the reciprocal lattice vectors, $\omega_z/2\pi$ is the harmonic trap frequency along the direction perpendicular to the lattice plane, and $\phi_{ij} = \phi_i - \phi_j$ is the relative phase between two of the three lattice beams, for which we choose the wavelength $\lambda = 1064$ nm. In Eq. (1), we omit the offset term and the influence of the external trap frequencies in the xy plane for simplicity. Unless otherwise mentioned, the atoms were initially loaded to a lattice depth of $V_0 = 3.0E_R$, where $E_R = \hbar^2 k_L^2/2m$ is the recoil energy, $k_L = 2\pi/\lambda$ is the wave number, $\hbar$ is the Planck constant divided by 2π, and m is the mass of the ^{87}Rb atom. The Hubbard parameters are $U/h = 30.7$ Hz and $J_{\rm bare}/h = 26.9$ Hz, where U and $J_{\rm bare}$ are the on-site interaction and the nearest-neighbor tunneling, respectively. The external trap frequencies are $(\omega_x, \omega_y, \omega_z)/2\pi = (88, 150, 184)$ Hz.

After lattice loading, we increased phase modulation signals to shake the optical triangular lattice elliptically [Fig. 1(a)]. According to the Floquet theory, the effective tunnelings J and J' in the rotating frame obey the zeroth-order Bessel function of the first kind (see Supplemental Material for the details of lattice-shaking parameters and experimental sequence [26]). The effective tunnelings are $(J, J')/J_{\rm bare} = (-0.35, -0.35)$ for Sp1 and $(-0.35, 0.35)$ for Sp2 throughout this Letter. The modulation frequency $\Omega/2\pi = 1.2$ kHz was carefully chosen to avoid multiphoton interband excitations [26,27]. We also note that the crossed FORT depth after lattice loading had to be lowered as much as possible so that the evaporation of atoms heated by lattice shaking could work well [26,28]. We observed the interference patterns of atoms using in-plane time-of-flight (TOF) [29], where the triangular lattice potential was suddenly switched off, whereas the vertical lattice potential was ramped up so that the atomic cloud could expand within the layers. Atoms were typically split into three layers in the vertical lattice, and more than 60% of the atoms were populated in a target layer of imaging. The in-plane TOF was followed by (i) a sudden ramp-up of all the optical lattices to freeze-out atoms, (ii) selection of the target layer by the combination of microwave and B-field gradient, and (iii) fluorescence imaging using the Raman sideband cooling [30]. Figures 1(c) and 1(d) show single-shot and averaged images of atom distributions after 5 ms in-plane TOF. In the case of Sp1 and Sp2, where twofold chiral degeneracy exists, the symmetry-broken images are observed [7]. We also checked the statistical distribution of the chiral contrast χ, which is defined in Fig. 1(e). The histograms appear binary, indicating that symmetry breaking often happens. We took the data at a ramp-up time of 200 ms for Sp1 and 300 ms for Sp2 with the crossed FORT depth optimized for each frustrated phase [26]. The atom number n per tube in the shaken lattice differed in each phase because the loss rate during lattice shaking depends on the phase-modulation amplitudes. For example, in Sp2, the filling was $n \sim 6$. Since $U/n|J^{(\prime)}| \sim 0.5$, this experiment is conducted in the weak-interaction regime, where the system is mapped to the classical XY model [31].

In the following, we focus on the relaxation from F to Sp1 and Sp2 [see Fig. 2(a)]. To quantify the relaxation times, we

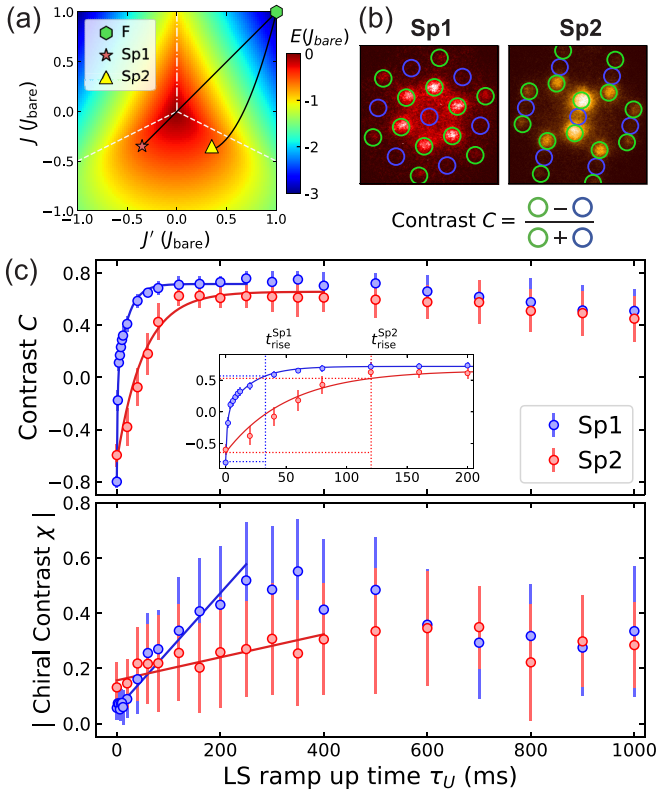

FIG. 2. Relaxation from F to Sp1 or Sp2. (a) Phase diagram of the classical XY model. The white dashed (dot-dashed) line means the phase transition of the 2nd (1st) order. The black solid lines represent the paths from F to Sp1 or Sp2. (b) Definition of contrast C. (c) C and $|\chi|$ with various ramp-up times of lattice shaking τ_U. Blue (red) points represent Sp1 (Sp2) data. Error bars denote standard deviations. The solid lines are fitting results to the data. The fitting function for C is defined in Eq. (2), while that for $|\chi|$ is a linear function with offset. The inset shows C from 0 to 200 ms ramp-up time together with the extracted rise times $t_{\text{rise}}^{\text{Sp1(2)}}$.

introduce contrast C defined in Fig. 2(b). When $C < 0$, the system is in an F state. $C > 0$ indicates a phase transition to Sp1 or Sp2. Figure 2(c) shows C and $|\chi|$ with various ramp-up times of the phase-modulation signals. The relaxation time of Sp1 is much shorter than that of Sp2. We made a fit to the data of C with our empirical exponential functions:

$$f(t) = \begin{cases} \frac{A}{2}(e^{-t/\tau_{\text{fast}}} + e^{-t/\tau_{\text{slow}}}) + B & \text{for Sp1,} \\ Ae^{-t/\tau} + B & \text{for Sp2,} \end{cases} \quad (2)$$

where A, B, τ, τ_{slow}, and τ_{fast} are fitting parameters. We define the rise time $t_{\text{rise}}^{\text{Sp1(2)}}$ such that $f(t_{\text{rise}}^{\text{Sp1(2)}}) = 0.1A + B$ is satisfied. The extracted rise times are $t_{\text{rise}}^{\text{Sp1}} = 32.9$ ms and $t_{\text{rise}}^{\text{Sp2}} = 120$ ms. We attribute this difference to two factors; one is the path length ratio after the phase transition over the total length [see black solid lines in Fig. 2(a)]. The ratio for Sp1 is 2.6 times larger than that for Sp2. The other is the effective band structures. In the tight-binding approximation, the energy difference between the ground states of Sp1 and the Γ point, at which a BEC is populated before lattice shaking, amounts to $\Delta E_{\Gamma}^{\text{Sp1}} = 3.6 J_{\text{bare}}$; on the other hand, the counterpart of Sp2 is $\Delta E_{\Gamma}^{\text{Sp2}} = 0.38 J_{\text{bare}}$, 9.5 times smaller [26]. A BEC at the Γ point becomes so unstable in Sp1 that it relaxes quickly into the true ground states. As for $|\chi|$, it strongly depends on the crossed FORT depths [26]. We note that the offset of $|\chi|$ in Sp2 data shifts upward since the regions of interest [blue and green circles in Fig. 1(e)] are close to the Γ points.

At a short ramp-up time of around 100 ms in Fig. 2(c), C is positive, which means that the phase transition has already happened. At the same time, $|\chi|$ is still small, which indicates that the simultaneous occupation of both chiral modes is observed more often than symmetry-broken images are. In a previous study [7], the possibility of domain formation was mentioned; however, this has yet to be confirmed. Therefore, we conducted an investigation to clarify this issue. The direct observation of chiral-mode domains in optical lattices was proposed in Ref. [32] assuming the far-field regime, which is difficult to reach in our system since the trap frequency limits in-plane TOF. Instead, we attempt to detect the formation of the chiral domains by observing the interference of spatially separated chiral modes.

Figures 3(a)–3(c) explain the processes from the domain formation to the observation of interference by the in-plane TOF. As shown in Fig. 3(a), the atoms in the optical triangular lattice and crossed FORTs have a shape elongated along the y axis. We assumed that during the ramp-up time a linear domain wall as shown in Fig. 3(b), which is the simplest of its kind, is formed most likely along the x axis because the domain wall energy is proportional to its length. During in-plane TOF, wave packets with different chiral modes interfere with each other. Consequently, interference fringes are observed. Figure 3(c) shows single-shot images of Sp1 and Sp2 with fringes and simulated images. To visualize the effect of fringes, we applied a fast Fourier transform (FFT) to the TOF images. Figure 3(d) shows the amplitude spectrum of the FFT images averaged over more than 100 runs. The spectrum spreads over along the y axis, which results from fringes. For comparison, the amplitude spectrum of F without lattice shaking is also shown. It appears symmetric, with no signs of fringes. We made a fit to the FFT signals to extract the widths along the long and short axes [26]. Figure 3(e) shows the histograms together with numerical simulation assuming various numbers of domain walls. While a single domain wall is dominant, multiple domain walls are sometimes formed in Sp2. Figure 3(f) shows the experimentally observed TOF image with multiple domain walls and the simulated image with $n_{\text{wall}} = 2$. In the FFT signals, we can see side peaks that result from interference of the same chiral modes.

Finally, the orientation of the domain wall was controlled using crossed FORTs. The trap frequencies in the xy plane are dominated by FORT 1 and FORT 2 [Fig. 3(a)], which have much tighter beam waists of 23 μm than the horizontal beam waists of the three beams that comprise the triangular lattice, ∼120 μm [30]. Therefore, the direction along which the atomic cloud is elongated depends on the intensity balance between FORT 1 and FORT 2. Figure 4(a) shows the atom distribution when the intensity of FORT 1, I_1, was much stronger than that of FORT2, I_2. The amplitude spectrum of the FFT in Sp2 is oriented in line with the atom distribution [Fig. 4(b)].

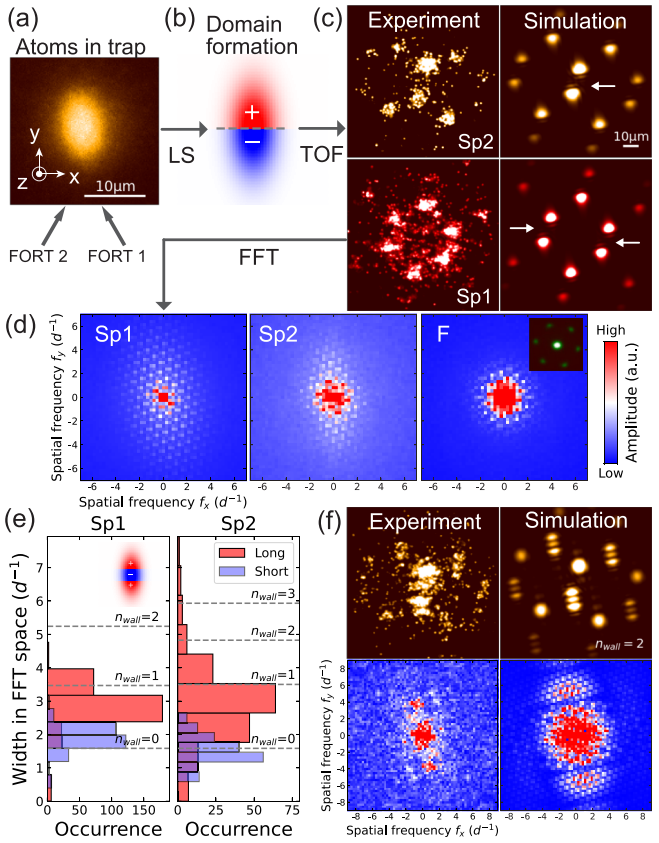

FIG. 3. Chiral-mode domains. (a) *In situ* image of atoms in the trap. The black arrows depict the directions along which the crossed FORTs are applied. The image is averaged over ten runs. (b) Schematic of domain formation. The dotted line at the center is a linear domain wall. (c) Experimentally observed (left) and simulated (right) TOF images. The ramp-up time of 70 and 80 ms was used for Sp1 and Sp2, respectively. In the right figure, the white arrows point to the region where the fringes appear, and the color scale is saturated at 0.3 times the maximum probability to emphasize the fringes. (d) Amplitude spectra of FFT for Sp1, Sp2, and F. The color scale is saturated at 0.2 times the maximum amplitude. $d = \frac{2}{3}\lambda$ in the axis labels means the lattice constant. FFT images are averaged for more than 100 runs. The inset shows the averaged TOF image of F as an icon. The distance of the inherent interference peaks is 1.18 d^{-1} in FFT space. (e) Histograms of the widths in FFT space. The red (blue) bars mean the widths along the long (short) axis. The dashed gray lines are the long-axis width estimated by the numerical simulation assuming the different number of walls n_{wall}. (f) TOF images that have multiple domain walls and their FFT signals. For better visibility, a Gaussian filter with $\sigma = 0.53\,d$ is applied to the experimentally observed TOF images in panels (c) and (f). The maximum and offset of the color scale of the experimental data in panels (c) and (f) are 0.4 times and 0.04 times the maximum FL count, respectively.

Figures 4(c) and 4(d) are the opposite case. Figure 4(e) compares the angles and widths in FFT space at different balances

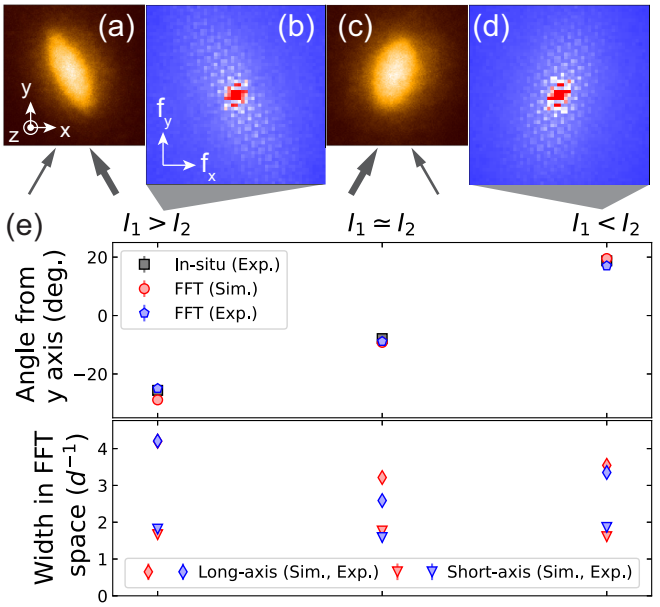

FIG. 4. Control of domain wall orientation. (a) Averaged *in situ* image of the atoms and (b) amplitude spectrum of FFT for TOF images in Sp2 under the condition $I_1 > I_2$. (c) and (d) Counterparts under the opposite condition $I_1 < I_2$. (e) Angles in *in situ* images and FFT space (upper row), and widths in FFT space (lower row) at different balances of FORTs. Error bars denoting fitting errors are covered with markers.

of FORTs. We can see good agreement between experiment and numerical simulation assuming $n_{\mathrm{wall}} = 1$.

In conclusion, we studied the relaxation from the ferromagnetic phase to two frustrated phases (Sp1 and Sp2) in the XY model on shaken optical triangular lattices. We revealed that domain walls [33–35] are formed in Sp1 and Sp2, which accounts for the simultaneous occupation of the two chiral modes. In this study, the system does not reach a strongly correlated regime. When the interaction is increased to $U/n|J| \gg 1$, one can access frustrated quantum magnetism, where the appearance of gapped spin-liquid phases is predicted [31]. The system can be mapped onto the spin-1 quantum XY model [36,37] near the Mott-insulating state with unit filling. In this situation, the quantum phase transition between the chiral superfluid and Mott insulator, where the symmetry of $\mathrm{U}(1) \times \mathbb{Z}_2$ is broken, can be investigated. Nonequilibrium dynamics after quenching across the phase transition and formation of domain structures can reveal the quantum Kibble-Zurek mechanism in this model [38].

We thank Daisuke Yamamoto for helpful discussions. This work was supported by JSPS KAKENHI Grants Nos. JP19H01854 and JP23H01133; the ImPACT Programme of Council for Science, Technology and Innovation (Cabinet Office, Government of Japan); and JST ERATO-FS Grant No. JPMJER2204.

[1] H. Diep, *Frustrated Spin Systems* (World Scientific, Singapore, 2004).

[2] R. Moessner and A. P. Ramirez, Geometrical frustration, Phys. Today **59**, 24 (2006).

[3] L. Balents, Spin liquids in frustrated magnets, Nature (London) **464**, 199 (2010).

[4] A. Harrison, First catch your hare: the design and synthesis of frustrated magnets, J. Phys.: Condens. Matter **16**, S553 (2004).

[5] K. Kim, M. S. Chang, S. Korenblit, R. Islam, E. E. Edwards, J. K. Freericks, G. D. Lin, L. M. Duan, and C. Monroe, Quantum simulation of frustrated Ising spins with trapped ions, Nature (London) **465**, 590 (2010).

[6] M. Qiao, Z. Cai, Y. Wang, B. Du, N. Jin, W. Chen, P. Wang, C. Luan, E. Gao, X. Sun, H. Tian, J. Zhang, and K. Kim, Observing frustrated quantum magnetism in two-dimensional ion crystals, arXiv:2204.07283.

[7] J. Struck, C. Ölschläger, R. Le Targat, P. Soltan-Panahi, A. Eckardt, M. Lewenstein, P. Windpassinger, and K. Sengstock, Quantum simulation of frustrated classical magnetism in triangular optical lattices, Science **333**, 996 (2011).

[8] J. Mongkolkiattichai, L. Liu, D. Garwood, J. Yang, and P. Schauss, Quantum gas microscopy of a geometrically frustrated Hubbard system, arXiv:2210.14895.

[9] M. Xu, L. H. Kendrick, A. Kale, Y. Gang, G. Ji, R. T. Scalettar, M. Lebrat, and M. Greiner, Frustration- and doping-induced magnetism in a Fermi–Hubbard simulator, Nature (London) **620**, 971 (2023).

[10] M. Lebrat, M. Xu, L. H. Kendrick, A. Kale, Y. Gang, P. Seetharaman, I. Morera, E. Khatami, E. Demler, and M. Greiner, Observation of Nagaoka polarons in a Fermi-Hubbard quantum simulator, arXiv:2308.12269.

[11] M. L. Prichard, B. M. Spar, I. Morera, E. Demler, Z. Z. Yan, and W. S. Bakr, Directly imaging spin polarons in a kinetically frustrated Hubbard system, arXiv:2308.12951.

[12] P. Scholl, M. Schuler, H. J. Williams, A. A. Eberharter, D. Barredo, K. N. Schymik, V. Lienhard, L. P. Henry, T. C. Lang, T. Lahaye, A. M. Läuchli, and A. Browaeys, Quantum simulation of 2D antiferromagnets with hundreds of Rydberg atoms, Nature (London) **595**, 233 (2021).

[13] G. Semeghini, H. Levine, A. Keesling, S. Ebadi, T. T. Wang, D. Bluvstein, R. Verresen, H. Pichler, M. Kalinowski, R. Samajdar, A. Omran, S. Sachdev, A. Vishwanath, M. Greiner, V. Vuletić, and M. D. Lukin, Probing topological spin liquids on a programmable quantum simulator, Science **374**, 1242 (2021).

[14] A. D. King, C. Nisoli, E. D. Dahl, G. Poulin-Lamarre, and A. Lopez-Bezanilla, Qubit spin ice, Science **373**, 576 (2021).

[15] R. Cosmic, K. Kawabata, Y. Ashida, H. Ikegami, S. Furukawa, P. Patil, J. M. Taylor, and Y. Nakamura, Probing XY phase transitions in a Josephson junction array with tunable frustration, Phys. Rev. B **102**, 094509 (2020).

[16] S. Teitel and C. Jayaprakash, Phase transtions in frustrated two-dimensional XY models, Phys. Rev. B **27**, 598 (1983).

[17] S. Miyashita and H. Shiba, Nature of the phase transition of the two-dimensional antiferromagnetic plane Rotator model on the triangular lattice, J. Phys. Soc. Jpn. **53**, 1145 (1984).

[18] D. H. Lee, J. D. Joannopoulos, J. W. Negele, and D. P. Landau, Discrete-symmetry breaking and novel critical phenomena in an antiferromagnetic planar (XY) model in two dimensions, Phys. Rev. Lett. **52**, 433 (1984).

[19] F. F. Song and G. M. Zhang, Tensor network approach to the two-dimensional fully frustrated XY model and a chiral ordered phase, Phys. Rev. B **105**, 134516 (2022).

[20] T. Obuchi and H. Kawamura, Spin and chiral orderings of the antiferromagnetic XY model on the triangular lattice and their critical properties, J. Phys. Soc. Jpn. **81**, 054003 (2012).

[21] J. P. Lv, T. M. Garoni, and Y. Deng, Phase transitions in XY antiferromagnets on plane triangulations, Phys. Rev. B **87**, 024108 (2013).

[22] A. Eckardt, Colloquium: Atomic quantum gases in periodically driven optical lattices, Rev. Mod. Phys. **89**, 011004 (2017).

[23] F. Wang, F. Pollmann, and A. Vishwanath, Extended supersolid phase of frustrated hard-core bosons on a triangular lattice, Phys. Rev. Lett. **102**, 017203 (2009).

[24] H. C. Jiang, M. Q. Weng, Z. Y. Weng, D. N. Sheng, and L. Balents, Supersolid order of frustrated hard-core bosons in a triangular lattice system, Phys. Rev. B **79**, 020409(R) (2009).

[25] D. Heidarian and A. Paramekanti, Supersolidity in the triangular lattice spin-1/2 XXZ model: A variational perspective, Phys. Rev. Lett. **104**, 015301 (2010).

[26] See Supplemental Material at http://link.aps.org/supplemental/10.1103/PhysRevResearch.5.L042026 for the theoretical and experimental details, which includes Refs. [7,22,27,28,39–43].

[27] M. Weinberg, C. Ölschläger, C. Sträter, S. Prelle, A. Eckardt, K. Sengstock, and J. Simonet, Multiphoton interband excitations of quantum gases in driven optical lattices, Phys. Rev. A **92**, 043621 (2015).

[28] M. Reitter, J. Näger, K. Wintersperger, C. Sträter, I. Bloch, A. Eckardt, and U. Schneider, Interaction dependent heating and atom loss in a periodically driven optical lattice, Phys. Rev. Lett. **119**, 200402 (2017).

[29] W. S. Bakr, A. Peng, M. E. Tai, R. Ma, J. Simon, J. I. Gillen, S. Fölling, L. Pollet, and M. Greiner, Probing the superfluid-to-Mott insulator transition at the single-atom level, Science **329**, 547 (2010).

[30] R. Yamamoto, H. Ozawa, D. C. Nak, I. Nakamura, and T. Fukuhara, Single-site-resolved imaging of ultracold atoms in a triangular optical lattice, New J. Phys. **22**, 123028 (2020).

[31] A. Eckardt, P. Hauke, P. Soltan-Panahi, C. Becker, K. Sengstock, and M. Lewenstein, Frustrated quantum antiferromagnetism with ultracold bosons in a triangular lattice, Europhys. Lett. **89**, 10010 (2010).

[32] A. Kosior and K. Sacha, Condensate phase microscopy, Phys. Rev. Lett. **112**, 045302 (2014).

[33] C. V. Parker, L.-C. Ha, and C. Chin, Direct observation of effective ferromagnetic domains of cold atoms in a shaken optical lattice, Nat. Phys. **9**, 769 (2013).

[34] T. Kock, M. Ölschläger, A. Ewerbeck, W.-M. Huang, L. Mathey, and A. Hemmerich, Observing chiral superfluid order by matter-wave interference, Phys. Rev. Lett. **114**, 115301 (2015).

[35] X.-Q. Wang, G.-Q. Luo, J.-Y. Liu, G.-H. Huang, Z.-X. Li, C. Wu, A. Hemmerich, and Z.-F. Xu, Observation of nematic orbital superfluidity in a triangular optical lattice, Phys. Rev. Lett., arXiv:2211.05578.

[36] E. Altman and A. Auerbach, Oscillating superfluidity of bosons in optical lattices, Phys. Rev. Lett. **89**, 250404 (2002).

[37] D. Yamamoto, T. Fukuhara, and I. Danshita, Frustrated quantum magnetism with Bose gases in triangular optical lattices at negative absolute temperatures, Commun. Phys. **3**, 56 (2020).

[38] A. Keesling, A. Omran, H. Levine, H. Bernien, H. Pichler, S. Choi, R. Samajdar, S. Schwartz, P. Silvi, S. Sachdev, P. Zoller, M. Endres, M. Greiner, V. Vuletić, and M. D. Lukin, Quantum Kibble–Zurek mechanism and critical dynamics on a

programmable Rydberg simulator, Nature (London) **568**, 207 (2019).

[39] N. Goldman and J. Dalibard, Periodically driven quantum systems: Effective Hamiltonians and engineered gauge fields, Phys. Rev. X **4**, 031027 (2014).

[40] X. Guo, W. Zhang, Z. Li, H. Shui, X. Chen, and X. Zhou, Asymmetric population of momentum distribution by quasi-periodically driving a triangular optical lattice, Opt. Express **27**, 27786 (2019).

[41] S. Arlinghaus and M. Holthaus, Driven optical lattices as strong-field simulators, Phys. Rev. A **81**, 063612 (2010).

[42] J.-P. Martikainen, Dynamical instability and loss of *p*-band bosons in optical lattices, Phys. Rev. A **83**, 013610 (2011).

[43] S. Paul and E. Tiesinga, Formation and decay of Bose-Einstein condensates in an excited band of a double-well optical lattice, Phys. Rev. A **88**, 033615 (2013).